Technique for sensitive carbon depth profiling in thin samples using C–C elastic scattering

Iva Bogdanović Radović,*[a] Milko Jakšić[a] and Francois Schiettekatte[b]

Received 18th June 2008, Accepted 14th November 2008
First published as an Advance Article on the web 5th December 2008
DOI: 10.1039/b810316j

A technique for carbon depth profiling in thin samples is described. It is developed to analyze low concentrations of carbon in heavier matrices. The method is based on the carbon–carbon elastic scattering coincidence measurement. Recoiled carbon atoms as well as scattered carbon ions from the primary beam are detected by two solid state detectors placed symmetrically at 45° around the beam direction. Since scattering products are detected in the forward direction, the method can be applied only for transmission samples with thicknesses of the order of several micrometers. Capabilities of the technique concerning depth resolution and sensitivity were tested on samples with known composition and depth distribution of carbon.

Introduction

Carbon is an element that is the main constituent of several materials such as organic matter. However, it can be presented as a trace element in several other materials while having a strong influence on the mechanical, electrical and other properties of metals, semiconductors and insulators. A typical case is carbon in steel where steel properties are strongly governed by the carbon concentration it contains. Steel with low carbon content has the same properties as iron. As carbon content rises, the metal becomes harder and stronger but less ductile and more difficult to weld. High carbon content lowers the steel melting point and its temperature resistance in general. Another example is the carbon content in semiconductor layers grown by metal-organic vapor phase epitaxy and used for the production of optoelectronic devices. Although diluted and electrically neutral, carbon can contribute to the formation of point defect complexes that will modify the material's optical and electronic properties.

Carbon analysis using optical methods such as infrared spectroscopy is restricted to a limited number of materials and a selection of carbon containing molecules. Raman and confocal μ-Raman spectroscopy are sensitive techniques for carbon detection, but the detection limit strongly depends on the sample type. Elemental carbon content can be quantitatively profiled by microanalysis techniques like Secondary Ion Mass Spectroscopy (SIMS) and Scanning Electron Microscope Energy Dispersive X-ray Spectroscopy (SEM EDX).[1,2] SIMS is a widespread depth profiling technique with very good sensitivity for carbon analysis. However, it is a destructive technique having rather limited depth range, while the quantification of analytical results is difficult due to large matrix effects. SEM EDX microanalysis on the other side has limited sensitivity for carbon analysis due to a small X-ray fluorescence yield and high peak to background ratio with even more restricted possibilities for measurements of carbon distribution at the sub-micrometer level.

The choice of the Ion Beam Analysis (IBA) technique is mainly governed by the amount as well as depth distribution of carbon in the sample. For materials where carbon is present in relatively large amounts (few at% or more), non-Rutherford backscattering analysis with protons or alpha particles can be successfully applied using the fact that excitation functions have energy regions with enhanced cross section (compared to Rutherford cross section) or narrow, sharp resonances. In the case of plateaus with enhanced cross sections only one measurement per sample is required to obtain a complete carbon depth profile. In the case of resonances, multiple measurements together with well calibrated accelerator energy are needed. For analysis of lower amounts of carbon in heavy matrix samples, the nuclear reaction $^{12}C(d,p)^{13}C$ is frequently used. Another technique frequently used for carbon profiling is Heavy Ion Elastic Recoil Detection Analysis (HI ERDA), but it can usually be applied only for determination of carbon content in the near surface (the first hundred nanometers). Since heavy ion beams are involved, such as ^{37}Cl or ^{127}I, beam-induced damage can be significant.

Cross-sections for scattering of different ions on C and estimated depth resolution near the sample surface for some typically used experimental setups are given in Table 1. We consider as an example a 3 μm thick SiO_2 target with low concentration of C (1 at%) homogeneously distributed inside the target. With $^{12}C(p,p)^{12}C$ elastic backscattering, such a small amount of C can be detected only if the resonance at 1.7 MeV is applied, however the energy resolution is not sufficient to measure the variation of C content inside the layer. If we use 4 MeV alphas, the depth resolution will improve due to the larger stopping, but the cross section is low and the C signal is again overlapped by the very large O signal. The resonance at 4.2 MeV can be applied, but enhances the cross section over a relatively small depth region and therefore multiple measurements are required. In the case of the $^{12}C(d,p)^{13}C$ reaction, typically a 1 MeV d beam is used for the analysis. Although the $^{12}C(d,p)^{13}C$ reaction is a background free method for C detection, the main drawback is a very small cross

[a]*Department for Experimental Physics, Ruđer Bošković Institute, P.O. Box 180, 10002 Zagreb, Croatia. E-mail: iva@irb.hr; Fax: +385 1 4680 239; Tel: +385 1 4571 227*
[b]*Regroupement Québécois sur les Matériaux de Pointe, Département de Physique, Université de Montréal, Montréal, QC, Canada H3C 3J7. E-mail: francois.schiettekatte@umontreal.ca; Fax: +1 514 343-7357; Tel: +1 514 343-6049*

Table 1 Cross section and estimated depth resolution near the sample surface for different reactions on C in a SiO_2 matrix

Beam/reaction	σ (mb/sr)	Δx (nm)
1.8 MeV p/^{12}C(p,p) ^{12}C	800 (at the 1.7 MeV resonance)	600
4 MeV α/^{12}C(α,α)^{12}C	62	140
1 MeV d	30	550
20 MeV Cl TOF ERDA	4575	17
12 MeV C–C	1610	100

section (at 1 MeV, only 30 mb/sr (millibarn per steradian)).[3] Deuterium beams also induce activation and neutron fluxes that many laboratories try to avoid. HI ERDA such as ERDA with 20 MeV ^{35}Cl ions is characterized with superior depth resolution. However a sophisticated spectrometer is required in order to distinguish the different masses such as time-of-flight (TOF) or ΔE–E detector. But more importantly, the depth that can be analyzed is typically in the range of 100 nm and depth resolution is drastically degraded with depth, so HI ERDA can only be applied for near surface layers.

Elastic coincidence scattering was first introduced by Cohen *et al.*[4] for detection of ppm amounts of hydrogen in metallic foils using 17 MeV protons. This technique was adapted later on to nuclear microprobes with lower[5,6] and higher[7] proton beam energies. Several authors have explored the use of coincidence scattering techniques for some other ion-atom systems. Moore *et al.*[8] have applied a 15–20 MeV ^{16}O beam to detect ^{16}O and ^{24}Mg impurities in nickel films and 40 MeV ^{35}Cl beams to detect ^{39}K and ^{63}Cu in gold. Smidt and Pieper have applied alpha–alpha scattering to measure the ^{4}He concentration profiles in thin metal films.[9] Hoffsäs *et al.*[10] have used a 2 MeV He beam to demonstrate profiling of carbon and oxygen in 2 μm thick self-supporting polycarbonate foils ($C_{16}O_3H_{14}$). In further experiments, boron and the surface oxygen of thin B doped Si crystal were also investigated.

In this paper we show how elastic scattering coincidence can be applied to depth profile carbon (here down to 0.06 at%) in heavier matrices. Carbon detection is performed by means of the elastic scattering of a high energy carbon beam on carbon nuclei in the target. As most events result from carbon scattering on other constituents in the target, a selection of carbon–carbon scattering events is obtained by coincident detection of two carbons emitted under a relative angle of 90° within the scattering plane. As we are detecting recoiled and scattered carbons in the forward direction (transmission geometry) it is clear that the maximum analyzable sample thickness depends on the carbon energy that can be delivered from the accelerator as well as on the stopping power of carbon ions in the material. The sensitivity, depth resolution and the effect of multiple scattering on the measurements is discussed.

Experiment

All measurements where performed on the 6 MV Tandem accelerator at the Ruđer Bošković Institute in Zagreb. ^{12}C ions were extracted from the sputtering ion source using a pure solid graphite target. In the experimental chamber, two surface-barrier particle detectors were placed at 45° forward angles

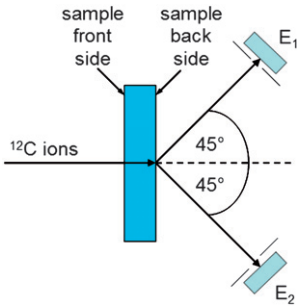

Fig. 1 Schematic drawing of the coincident C–C elastic scattering configuration.

symmetrically to the beam direction as is shown at Fig. 1. Collimating apertures were fitted to each detector so that solid angles of both detectors were 3 msr, which corresponds to an angular distribution of 45° ± 2°. The data acquisition system was controlled by the SPECTOR program.[11]

After an event in which the carbon ion hits a carbon from the target, two identical particles are emitted at an angle of 90° relative to each other in the laboratory frame. Carbon signals from both detectors are summed. To distinguish those two signals from the rest of the scattering events that can happen in the target, the bipolar signals from each detector amplifiers were used to produce a coincidence condition. A coincidence window of a few nanoseconds significantly reduces background coming from scattering of carbon from other target constituents even at high counting rates (~10^4 counts/s) which is necessary for low concentration measurements in a reasonable amount of time. For our geometry and angle opening, coincidence detection is fulfilled only for C–C elastic scattering. The coincidence time analyzer was set so that only signals which fall within a 13 ns time window were further processed. Those signals were used for gating the unipolar output from both amplifiers which were added together. In addition, as transmission targets were used, the beam charge measured by a Faraday cup was recorded. The maximal possible target thickness that can be investigated is determined by the ^{12}C ion energy. For 5 μm thick SiO_2 samples, the beam energy should be at least 18 MeV to get information from all depths in the sample as can be seen using SRIM.[12] From all this it is clear that the method is applicable only to samples that can be prepared as self supporting thin films.

Cross sections

The scattering of identical particles in the forward direction results in a quantum-mechanical interference term and is described by Mott scattering. From ref. 13 it is seen that below the Coulomb barrier, which is around 13 MeV for elastic C–C scattering, experimental data are in an agreement with Mott formula. Around $\theta_{lab} = 45°$ ($\theta_{cm} = 90°$), this cross section is symmetric and larger than the Rutherford cross section. For 12 MeV ^{12}C ions and $\theta_{lab} = 45°$, the Mott cross section gives 1.61 b/sr that is three times larger than the Rutherford cross section. At energies above the Coulomb barrier the excitation curves and angular distribution near $\theta_{lab} = 45°$ show a decrease in cross section below the Mott predictions and can be predicted by the Blair model.[13] However, the reduction in elastic cross

section as well as possible overlapping of the elastic scattering channel with the cross sections for different inelastic channels makes C–C scattering at higher carbon ion energies more difficult.

Results and discussion

The method is studied against two important parameters: depth resolution and sensitivity. The depth resolution δx is the ability to separate, in the spectrum along the energy axis, the signal contribution from atoms at different depths in the sample and is defined as[14]

$$\delta x = \frac{\delta E_d}{S_{eff}} \quad (1)$$

where δE_d is the total energy resolution and S_{eff} is the effective stopping power defined as

$$S_{eff} = \frac{kS_1}{\cos\theta_1} + \frac{S_2}{\cos\theta_2} \quad (2)$$

where k is the kinematic factor and is equal to $\cos^2\theta_2$ for scattering of identical particles, θ_1 is the angle between incident beam and target normal (in our case 0°), θ_2 is the scattering angle (here 45°±2°), and S_1 and S_2 are the stopping powers of incident and scattered beam in the material, respectively.

There are several factors contributing to the overall energy resolution such as: particle detector energy resolution, energy and angular spread of the beam, geometrical spread caused by finite beam spot size and detector solid angle, straggling of incident ions and emitted particles in the target and the multiple scattering of incident ions and emitted particles. The relative intrinsic energy resolution of used silicon detectors for C ions was measured to be ~150 keV for 6 MeV ions. The beam spread of the primary energy was 0.1% (12 keV for 12 MeV ^{12}C ions). Taking into account that we record the sum energy of two coincident ions instead of single ion energy, first order kinematic spread due to finite solid angle opening is reduced to 0 at the sample side away from the incident beam (back side at Fig. 1). The effect is shown at Fig. 2 for the case of a thin C foil (20 μg/cm^2). Fig. 2a and 2b show coincidence energy spectra from energy detector E_1 and E_2 respectively, while Fig. 2c displays half of the sum energy from both detectors $(E_1 + E_2)/2$. At the sample side facing the incident beam (front side at Fig. 1), the contribution coming from the kinematic spread is not completely canceled, especially for thicker samples, due to the differences in paths of outgoing C atoms through the sample. However, this contribution is about 25 keV for a 3 μm thick Mylar foil, which is small compared to the detector energy resolution.

Programs usually used for estimating depth resolution contributions such as Depth[15] or SIMNRA[16] are not suited for calculating depth resolution for the coincidence detection of identical scattered and recoiled particles. Therefore, the Monte Carlo simulation code CORTEO[17] was modified to properly account for coincidence scattering. In addition to computing the trajectories of incoming and scattered ions, it computes the trajectory of the recoil, and its intersection with one of the detectors. It thus correctly accounts for the effect of multiple collisions on the detection efficiency. In addition to multiple

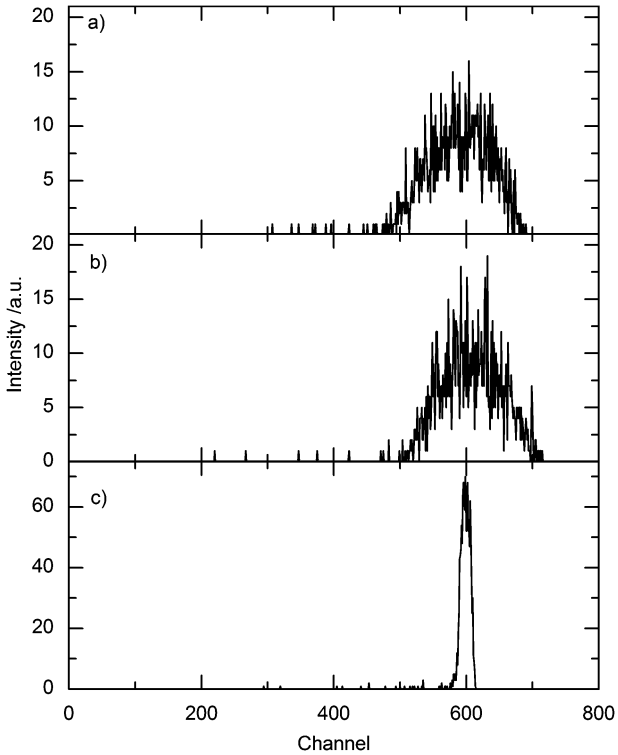

Fig. 2 Coincidence energy spectra a) E_1 detector, b) E_2 detector, c) $(E_1 + E_2)/2$.

scattering, CORTEO namely takes into account energy straggling and geometrical effects. CORTEO was used for calculating the theoretical depth resolution as well as for comparing experimental results with theoretical predictions. Theoretical predictions for depth resolution for carbon at the front and back side of thin Mylar® sample irradiated with 12 MeV ^{12}C ions as a function of the sample thickness are displayed in Fig 3. From this figure, it is clear that better depth resolution can be expected at the back side of the sample. Therefore it is important to place structures that we want to investigate closer to the back side. Also, above some particular thickness (in the case of Mylar® ~ 3 μm) depth resolution at the front side starts to deteriorate rapidly.

The method was tested with thin samples containing different amounts of C. To set the coincidence window, we irradiated 20 μg/cm^2 (88 nm) thick pure C foil. The resulting spectrum is shown at Fig. 2c. A 3 μm thick Mylar® covered with 88 nm C foil was used as a standard containing a known amount of C. The C layer was directed to the beam to improve heat and charge conductivity and reduce beam damage effects to the polycarbonate foil. In Mylar®, the C concentration (45 at%) is homogeneously distributed along the sample depth. Therefore, this foil is perfect to study the number of lost coincidence events as a function of depth in the sample due to scattering. The C–C coincidence spectrum from the 3 μm thick Mylar® foil together with the 2D energy-time map is shown on Fig. 4. The spectrum is narrow at the high energy side and becomes broader and less well defined in time for events occurring closer to the sample side facing the beam due to multiple scattering of outgoing scattered and recoiled C ions inside the sample. Depth profiles can be obtained by projecting scattering events to the energy axis. The

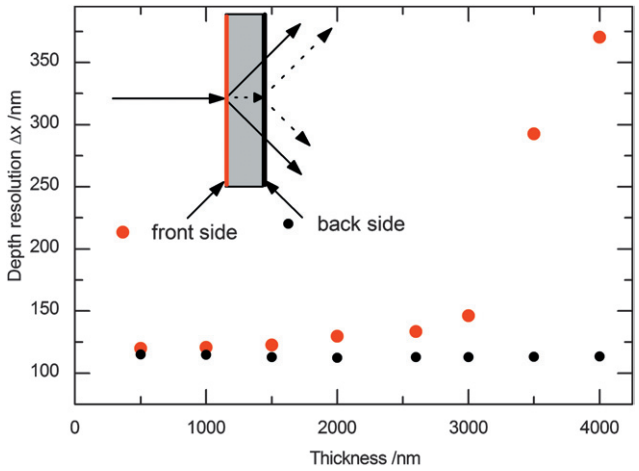

Fig. 3 Depth resolution at the front and back side of the Mylar® as a function of sample thickness for the 12 MeV ^{12}C beam.

experimental spectrum was compared with two simulation programs: SIMNRA[16] which is not optimized for coincident scattering and the version of CORTEO modified for coincident scattering of identical particles. As it can be seen from Fig. 4b, the simulations differ in the low energy part of the spectrum. This

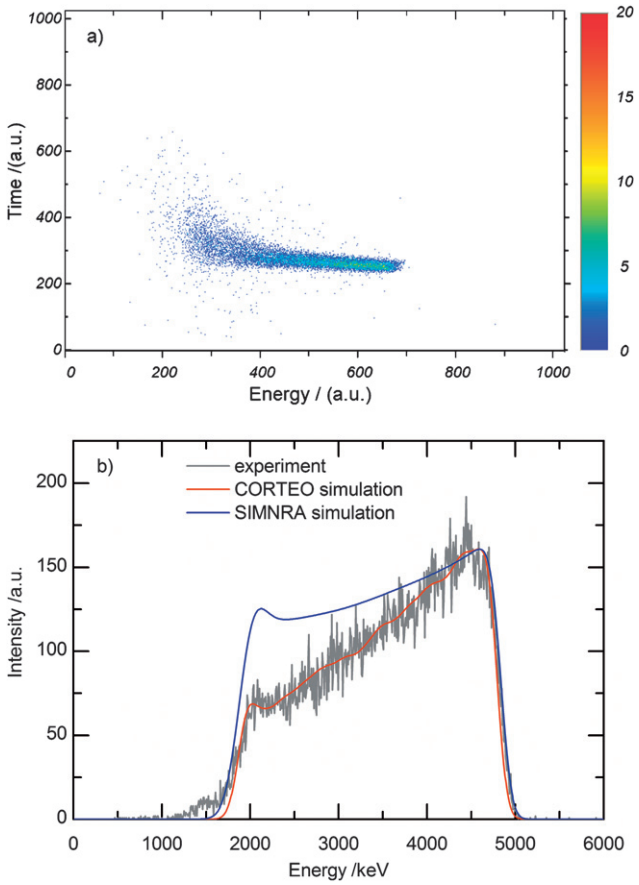

Fig. 4 a) Two dimensional map of coincident C–C scattering events from 3 μm thick Mylar® foil *vs.* coincidence time, b) projection to the energy axis.

is caused by the loss of true coincidence events due to multiple scattering. Multiple scattering depends on target material as well as ion energy and total energy loss while traveling through the material. Therefore, an ion pair produced by scattering near the front surface of the sample will be more influenced by this effect since the trajectory of both particles, supposed to cross the material towards the detectors, will be affected independently by multiple scattering, increasing the probability that the event escapes detection. From Fig. 4b can be seen that the Monte Carlo code can interpret correctly amplitude decrease with energy caused by multiple scattering if we take into account realistic detector solid angles.

The experimental energy resolution was calculated by fitting the edge of the energy profile with a Boltzman function. At the back side total dispersion in energy was 245 keV. For the front side of the sample, the energy spread was 288 keV, which is expected because all effects are more pronounced for ions that after the scattering event need to travel through total sample thickness before being detected. As it can be seen from Fig. 4b, there is a little bump in the low energy part of the spectrum. One possible explanation may be that this bump is due to the change in the sample thickness that occurs during the irradiation of Mylar foil with the ^{12}C beam. Irradiation with carbon ions makes the sample thinner due to the beam induced damage. By getting thinner, the entire coincident spectrum is shifted toward the higher energies, but the effect can be only seen at the low energy side of the spectrum. S_{eff} was calculated from ref. 16 to be 0.215 keV/10^{15} at cm^{-2} at the back side which leads to a depth resolution of 119 nm. The obtained depth resolution is in good agreement with the CORTEO simulation.

As an example of sample containing a small amount of carbon, we implanted 1 MeV C ions into a 2 μm thick Al foil. The implanted fluence was 1.3×10^{16} C/cm^2. The implantation profile was calculated using the Monte Carlo simulation program SRIM.[12] According to the simulation, the maximum concentration of implanted C (~0.8 at%) is expected at the depth of 1.4 μm with FWHM of the implanted peak of 202 nm. During the C–C coincident measurement, foil was oriented towards the ion beam the same way as it was during implantation (implantation peak closer to the sample back side). To estimate the contribution of accidental coincidences and the method sensitivity, spectrum from a 2 μm thick pure Al foil was collected under the same experimental conditions and for the same number of impinging ions. Both spectra are shown in Fig. 5. At both foil surfaces, a strong C signal is visible for both implanted and non-implanted foil due to the surface contamination by organic material. In the implanted foil, a peak corresponding to implanted C is also visible. The FWHM of the implanted peak from the C–C experiment is calculated to be 356 nm. The depth resolution was estimated from widths of surface peaks at both sides of the foil. Taking into account S_{eff} in thin organic layers and assuming that they are very thin, it was calculated that $\Delta x_{back} = 149$ nm and $\Delta x_{front} = 230$ nm. The peak coming from implanted C at depth 1.4 μm in the sample can be well separated from the surface contamination peaks as can be seen in Fig. 5.

The sensitivity of the method was estimated from the number of background counts N_B in pure Al foil in the region where the implanted peak is located. Assuming that the Al foil is carbon free and taking into account that the minimum detection

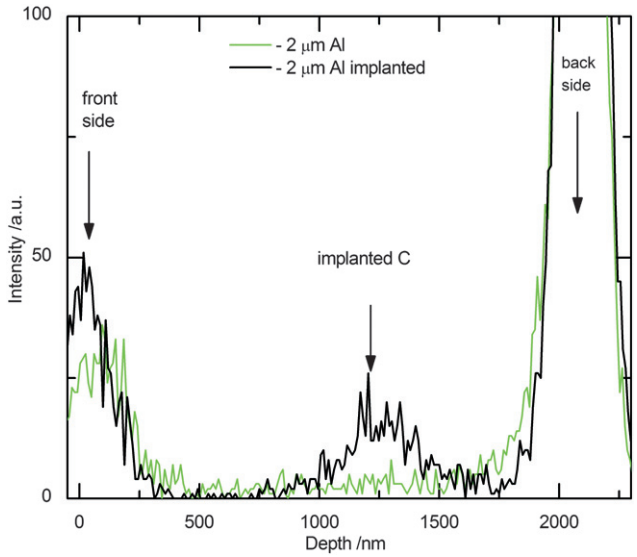

Fig. 5 Coincident C–C elastic scattering spectra of the pure and C implanted 2 μm thick Al foil.

limit (MDL) is given as $3\sqrt{N_B}$ we obtain a sensitivity of $\sim 1 \times 10^{15}$ at/cm^2, which corresponds to about ~600 ppm of C in the maximum of the implantation peak. It is important to mention that this sensitivity is obtained with rather small detector solid angles of only 3 msr.

Conclusions

The C–C coincidence scattering method has been demonstrated to be an effective technique for detection of low amounts of C in thin, transmission samples. The features of the spectrum, such as the depth resolution and the detection efficiency as a function of depth are well reproduced by a simulation which properly accounts for multiple scattering, energy straggling and geometrical effects. With relatively small detector solid angles, we obtained a detection limit of 600 ppm for C in Al with a depth resolution around 150 nm which is significantly better than for other typically used ion beam analysis methods. Due to the canceling of first order kinematic spread for identical particles, detectors with two to three orders of magnitude larger solid angles can be applied (like the annular silicon strip detector used in ref. 7) and ppm sensitivity in C detection can be achieved.

References

1 A. Pérez-Rodríguez, A. Cornet and J. R. Morante, *Microelectronic Engineering*, 1998, **40**, 223.
2 Xiaolin Hou and Per Roosa, *Analytica Chimica Acta*, 2008, **608**, 105.
3 E. Kashy, R. R. Perry and J. R. Risser, *Phys. Rev.*, 1960, **117**, 1289.
4 B. L. Cohen, C. L. Fink and J. H. Degnan, *J. Appl. Phys.*, 1972, **43**, 19.
5 D. Dujmić, M. Jakšić, N. Soić, T. Tadić and I. Bogdanović, *Nucl. Instrum. Methods Phys. Res., Sect. B*, 1996, **111**, 126.
6 K. A. Sjöland, P. Kristiansson, M. Elfman, K. G. Malmqvist, J. Pallon, R. J. Utui and C. Yang, *Nucl. Instrum. Methods Phys. Res., Sect. B*, 1997, **124**, 639.
7 P. Reichart, G. Dollinger, A. Bergmaier, G. Datzmann, A. Hauptner and H.-J. Körner, *Nucl. Instrum. Methods Phys. Res., Sect. B*, 2002, **197**, 134.
8 J. A. Moore, I. V. Mitchell, M. J. Hollis, J. A. Davies and L. M. Howe, *J. Appl. Phys.*, 1975, **46**, 52.
9 F. A. Smidt Jr. and A. G. Pieper, *J. Nucl. Mater.*, 1974, **51**, 361.
10 H. C. Hofsäss, N. R. Parikh, M. L. Swanson and W. K. Chu, *Nucl. Instrum. Methods Phys. Res., Sect. B*, 1991, **58**, 49.
11 M. Bogovac, I. Bogdanović, S. Fazinić, M. Jakšić, L. Kukec and W. Wilhelm, *Nucl. Instrum. Methods Phys. Res., Sect. B*, 1994, **89**, 219.
12 J. F. Ziegler, *Nucl. Instrum. Methods Phys. Res., Sect. B*, 2004, **219**, 1027.
13 D. A. Bromley, J. A. Kuehner and E. Almquist, *Phys. Rev.*, 1961, **123**, 878.
14 J. A. Leavitt and L. C. McIntyre Jr., in *Handbook of Modern Ion Beam Materials Analysis*, ed. J. R. Tesmerand M. Nastasi, Materials Research Society, Pittsburg, 1st edn., 1995, (ch. 4), pp. 39–81.
15 E. Szilágyi, F. Pászti and G. Amsel, *Nucl. Instrum. Methods Phys. Res., Sect. B*, 1995, **100**, 103.
16 M. Mayer, *Technical Report IPP 9/113*, Max-Planck Institut fur Plasmaphysik, Garching, Germany, 1997.
17 F. Schiettekatte, *Nucl. Instrum. Methods Phys. Res., Sect. B*, 2008, **266**, 1880.